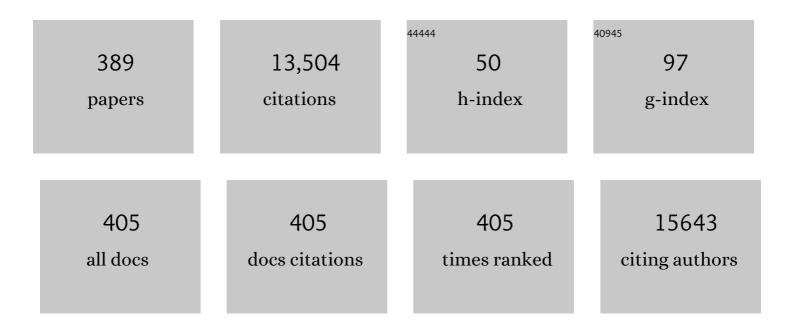
List of Publications by Year in descending order

Source: https://exaly.com/author-pdf/3109413/publications.pdf Version: 2024-02-01



#	Article	IF	CITATIONS
1	Recent Progress on Mixed-Anion Materials for Energy Applications. Bulletin of the Chemical Society of Japan, 2022, 95, 26-37.	2.0	51
2	Anion Substitution at Apical Sites of Ruddlesden–Popper-type Cathodes toward High Power Density for All-Solid-State Fluoride-Ion Batteries. Chemistry of Materials, 2022, 34, 609-616.	3.2	13
3	Multiscale and hierarchical reaction mechanism in a lithium-ion battery. Chemical Physics Reviews, 2022, 3, .	2.6	11
4	Studies on the inhibition of lithium dendrite formation in sulfide solid electrolytes doped with LiX (XÂ=ÂBr, I). Solid State Ionics, 2022, 377, 115869.	1.3	15
5	Fast fluoride ion conduction of NH4(Mg1-xLix)F3-x and (NH4)2(Mg1-xLix)F4-x assisted by molecular cations. Scientific Reports, 2022, 12, 5955.	1.6	2
6	High Rate Capability from a Graphite Anode through Surface Modification with Lithium Iodide for All-Solid-State Batteries. ACS Applied Energy Materials, 2022, 5, 667-673.	2.5	15
7	Magnetic Compton Scattering Study of Li-Rich Battery Materials. Condensed Matter, 2022, 7, 4.	0.8	5
8	State of the Active Site in La <sub>1–<i>x</i></sub> Sr <sub><i>x</i></sub> CoO <sub>3â^Î</sub> Under Oxygen Evolution Reaction Investigated by Total-Reflection Fluorescence X-Ray Absorption Spectroscopy. ACS Applied Energy Materials, 2022, 5, 4108-4116.	2.5	4
9	Partial cation disorder in Li <sub>2</sub> MnO <sub>3</sub> obtained by high-pressure synthesis. Applied Physics Letters, 2022, 120, 182404.	1.5	0
10	Improvement of Visibleâ€Light H <sub>2</sub> Evolution Activity of Pb <sub>2</sub> Ti <sub>2</sub> O <sub>5.4</sub> F <sub>1.2</sub> Photocatalyst by Coloading of Rh and Pd Cocatalysts. Chemistry - A European Journal, 2022, 28, .	1.7	2
11	Rocksalt type Li2Nb0·15Mn0·85O3 without structure degradation or redox evolution upon cycling. Journal of Alloys and Compounds, 2021, 853, 156984.	2.8	4
12	Comparison of Sulfur Cathode Reactions between a Concentrated Liquid Electrolyte System and a Solid-State Electrolyte System by Soft X-Ray Absorption Spectroscopy. ACS Applied Energy Materials, 2021, 4, 186-193.	2.5	10
13	Understanding the reaction mechanism and performances of 3d transition metal cathodes for all-solid-state fluoride ion batteries. Journal of Materials Chemistry A, 2021, 9, 406-412.	5.2	33
14	Hydride-based antiperovskites with soft anionic sublattices as fast alkali ionic conductors. Nature Communications, 2021, 12, 201.	5.8	46
15	<i>Operando</i> X-ray Absorption Spectroscopic Study on the Effect of Ionic Liquid Coverage upon the Oxygen Reduction Reaction Activity of Pd-core Pt-shell Catalysts. Electrochemistry, 2021, 89, 31-35.	0.6	4
16	Kinetic analysis and alloy designs for metal/metal fluorides toward high rate capability for all-solid-state fluoride-ion batteries. Journal of Materials Chemistry A, 2021, 9, 7018-7024.	5.2	16
17	High Ionic Conductivity of Liquid-Phase-Synthesized Li <sub>3</sub> PS <sub>4</sub> Solid Electrolyte, Comparable to That Obtained via Ball Milling. ACS Applied Energy Materials, 2021, 4, 2275-2281.	2.5	33
18	Improvement of lithium ionic conductivity of Li3PS4 through suppression of crystallization using low-boiling-point solvent in liquid-phase synthesis. Solid State Ionics, 2021, 361, 115568.	1.3	21

#	Article	IF	CITATIONS
19	Compton Scattering Imaging of Liquid Water in Porous Carbon-Based Materials. Applied Sciences (Switzerland), 2021, 11, 3851.	1.3	3
20	Cu–Pb Nanocomposite Cathode Material toward Room-Temperature Cycling for All-Solid-State Fluoride-Ion Batteries. ACS Applied Energy Materials, 2021, 4, 3352-3357.	2.5	18
21	Impact of the Composition of Alcohol/Water Dispersion on the Proton Transport and Morphology of Cast Perfluorinated Sulfonic Acid Ionomer Thin Films. ACS Omega, 2021, 6, 14130-14137.	1.6	6
22	Tomographic reconstruction of oxygen orbitals in lithium-rich battery materials. Nature, 2021, 594, 213-216.	13.7	56
23	Rate-Determining Process at Electrode/Electrolyte Interfaces for All-Solid-State Fluoride-Ion Batteries. ACS Applied Materials & Interfaces, 2021, 13, 30198-30204.	4.0	14
24	Investigation of the Suppression of Dendritic Lithium Growth with a Lithium-Iodide-Containing Solid Electrolyte. Chemistry of Materials, 2021, 33, 4907-4914.	3.2	30
25	Mixed alkali-ion transport and storage in atomic-disordered honeycomb layered NaKNi2TeO6. Nature Communications, 2021, 12, 4660.	5.8	23
26	Quantitative Evaluation of the Activity of Low-Spin Tetravalent Nickel Ion Sites for the Oxygen Evolution Reaction. ACS Applied Energy Materials, 2021, 4, 10731-10738.	2.5	5
27	Probing the Dissolved Gas Concentration on the Electrode through Laser-Assisted Bubbles. Journal of Physical Chemistry C, 2021, 125, 20952-20957.	1.5	6
28	Phase Transition Behavior of MgMn <sub>2</sub> O <sub>4</sub> Spinel Oxide Cathode during Magnesium Ion Insertion. Chemistry of Materials, 2021, 33, 1006-1012.	3.2	24
29	<i>Operando</i> X-ray Absorption Spectroscopic Study on the Influence of Specific Adsorption of the Sulfo Group in the Perfluorosulfonic Acid Ionomer on the Oxygen Reduction Reaction Activity of the Pt/C Catalyst. ACS Applied Energy Materials, 2021, 4, 1143-1149.	2.5	15
30	Fluoride-Ion Shuttle Battery with High Volumetric Energy Density. Chemistry of Materials, 2021, 33, 459-466.	3.2	31
31	Reversible and Fast (De)fluorination of High apacity Cu <sub>2</sub> O Cathode: One Step Toward Practically Applicable All olidâ€State Fluorideâ€Ion Battery. Advanced Energy Materials, 2021, 11, 2102285.	10.2	23
32	Effect of Temperature on Oxygen Reduction Reaction Kinetics for Pd Core–Pt Shell Catalyst with Different Core Size. ACS Applied Energy Materials, 2021, 4, 810-818.	2.5	6
33	Accelerated lithium ions diffusion at the interface between LiFePO4 electrode and electrolyte by surface-nitride treatment. Solid State Ionics, 2021, 373, 115792.	1.3	2
34	The Effect of Cation Mixing in LiNiO 2 toward the Oxygen Evolution Reaction. ChemElectroChem, 2021, 8, 70-76.	1.7	4
35	(Invited) Operando X-Ray Absorption Fine Structure Studies of Polymer Electrolyte Membrane Electrolysis and Alkaline Water Electrolysis. ECS Meeting Abstracts, 2021, MA2021-02, 1276-1276.	0.0	0
36	Structural environment of chloride ionâ€conducting solids based on lanthanum oxychloride. Journal of the American Ceramic Society, 2020, 103, 297-303.	1.9	15

#	Article	IF	CITATIONS
37	Observation of Subsurface Structure of Pt/C Catalyst Using Pair Distribution Function and Simple Modeling Techniques. Bulletin of the Chemical Society of Japan, 2020, 93, 37-42.	2.0	5
38	Reviving Galvanic Cells To Synthesize Core–Shell Nanoparticles with a Quasi-Monolayer Pt Shell for Electrocatalytic Oxygen Reduction. ACS Catalysis, 2020, 10, 430-434.	5.5	11
39	Structural analysis of imperfect Li2TiO3 crystals. Journal of Alloys and Compounds, 2020, 819, 153037.	2.8	6
40	Charge Compensation Mechanism of Lithium-Excess Metal Oxides with Different Covalent and Ionic Characters Revealed by <i>Operando</i> Soft and Hard X-ray Absorption Spectroscopy. Chemistry of Materials, 2020, 32, 139-147.	3.2	37
41	Synthesis of Sulfide Solid Electrolytes through the Liquid Phase: Optimization of the Preparation Conditions. ACS Omega, 2020, 5, 26287-26294.	1.6	22
42	Relationship between rate performance and electronic/structural changes during oxygen redox of lithium-rich 4d/3d transition metal oxides. Solid State Ionics, 2020, 357, 115459.	1.3	6
43	Evaluation of oxygen contribution on delithiation process of Li-rich layered 3d transition metal oxides. Materials Today Communications, 2020, 25, 101673.	0.9	4
44	Substrate-dependent proton transport and nanostructural orientation of perfluorosulfonic acid polymer thin films on Pt and carbon substrate. Solid State Ionics, 2020, 357, 115456.	1.3	4
45	Effect of Interaction among Magnesium Ions, Anion, and Solvent on Kinetics of the Magnesium Deposition Process. Journal of Physical Chemistry C, 2020, 124, 28510-28519.	1.5	19
46	Nanostructured LiMnO <sub>2</sub> with Li <sub>3</sub> PO <sub>4</sub> Integrated at the Atomic Scale for High-Energy Electrode Materials with Reversible Anionic Redox. ACS Central Science, 2020, 6, 2326-2338.	5.3	22
47	Disordered Cubic Spinel Structure in the Delithiated Li <sub>2</sub> MnO <sub>3</sub> Revealed by Difference Pair Distribution Function Analysis. Journal of Physical Chemistry C, 2020, 124, 24081-24089.	1.5	8
48	Concentration profile of dissolved gas during hydrogen gas evolution: an optical approach. Chemical Communications, 2020, 56, 14483-14486.	2.2	10
49	Surface analysis of lanthanum strontium cobalt oxides under cathodic polarization at high temperature through operando total-reflection X-ray absorption and X-ray fluorescence spectroscopy. Solid State Ionics, 2020, 357, 115502.	1.3	7
50	Observation of Liquid Phase Synthesis of Sulfide Solid Electrolytes Using Timeâ€Resolved Pair Distribution Function Analysis. Physica Status Solidi (B): Basic Research, 2020, 257, 2070041.	0.7	0
51	Capacity Improvement by Nitrogen Doping to Lithium-Rich Cathode Materials with Stabilization Effect of Oxide Ions Redox. ACS Applied Energy Materials, 2020, 3, 4162-4167.	2.5	18
52	Determining Factor on the Polarization Behavior of Magnesium Deposition for Magnesium Battery Anode. ACS Applied Materials & Interfaces, 2020, 12, 25775-25785.	4.0	31
53	Structureâ€Activity Relationship in a Cobalt Aluminate Nanoparticle Cocatalyst with a Graphitic Carbon Nitride Photocatalyst for Visibleâ€Light Water Oxidation. ChemPhotoChem, 2020, 4, 5175-5180.	1.5	1
54	Enhanced Performance Induced by Phase Transition of Li <sub>2</sub> FeSiO <sub>4</sub> upon Cycling at High Temperature. ACS Applied Energy Materials, 2020, 3, 5722-5727.	2.5	7

#	Article	IF	CITATIONS
55	A reversible oxygen redox reaction in bulk-type all-solid-state batteries. Science Advances, 2020, 6, eaax7236.	4.7	34
56	Observation of Liquid Phase Synthesis of Sulfide Solid Electrolytes Using Timeâ€Resolved Pair Distribution Function Analysis. Physica Status Solidi (B): Basic Research, 2020, 257, 2000106.	0.7	4
57	Morphology Changes in Perfluorosulfonated Ionomer from Thickness and Thermal Treatment Conditions. Langmuir, 2020, 36, 3871-3878.	1.6	17
58	Influence of Active Material Loading on Electrochemical Reactions in Composite Solid-State Battery Electrodes Revealed by <i>Operando</i> 3D CT-XANES Imaging. ACS Applied Energy Materials, 2020, 3, 7782-7793.	2.5	29
59	Thickness-induced metal to insulator transition in Ru nanosheets probed by photoemission spectroscopy: Effects of disorder and Coulomb interaction. Scientific Reports, 2020, 10, 1541.	1.6	2
60	Water Oxidation through Interfacial Electron Transfer by Visible Light Using Cobalt-Modified Rutile Titania Thin-Film Photoanode. ACS Applied Materials & Interfaces, 2020, 12, 9219-9225.	4.0	12
61	Cobalt Aluminate Spinel as a Cocatalyst for Photocatalytic Oxidation of Water: Significant Hole-Trapping Effect. ACS Catalysis, 2020, 10, 4960-4966.	5.5	33
62	Activation of a Pt-loaded Pb <sub>2</sub> Ti <sub>2</sub> O <sub>5.4</sub> F <sub>1.2</sub> photocatalyst by alkaline chloride treatment for improved H <sub>2</sub> evolution under visible light. Journal of Materials Chemistry A, 2020, 8, 9099-9108.	5.2	11
63	Reaction mechanism of electrochemical insertion/extraction of magnesium ions in olivine-type FePO4. Solid State Ionics, 2020, 349, 115311.	1.3	8
64	3D <i>Operando</i> Imaging and Quantification of Inhomogeneous Electrochemical Reactions in Composite Battery Electrodes. Journal of Physical Chemistry Letters, 2020, 11, 3629-3636.	2.1	35
65	Single-shot laser-scattering technique refined for the real-time monitoring and sizing of individual nanoparticles and nanobubbles in bulk water. Optics Letters, 2020, 45, 3321.	1.7	Ο
66	<i>Operando</i> soft X-ray absorption spectroscopic study on microporous carbon-supported sulfur cathodes. RSC Advances, 2020, 10, 39875-39880.	1.7	8
67	Investigation of Cathodic Reaction Mechanism in Solid Oxide Fuel Cells by <i>Operando</i> X-Ray Absorption Spectroscopy. Electrochemistry, 2020, 88, 560-565.	0.6	3
68	Solar Water Oxidation by a Visibleâ€Lightâ€Responsive Tantalum/Nitrogenâ€Codoped Rutile Titania Anode for Photoelectrochemical Water Splitting and Carbon Dioxide Fixation. ChemPhotoChem, 2019, 3, 37-45.	1.5	34
69	Quantitative Elucidation of the Non-Equilibrium Phase Transition in LiFePO <sub>4</sub> via the Intermediate Phase. Chemistry of Materials, 2019, 31, 7160-7166.	3.2	22
70	Identification of ferrimagnetic orbitals preventing spinel degradation by charge ordering in <mml:math xmlns:mml="http://www.w3.org/1998/Math/MathML"&gt;<mml:mrow><mml:msub><mml:mi>Li</mml:mi><mml:r mathvariant="normal"&gt;O<mml:mn>4</mml:mn></mml:r </mml:msub></mml:mrow>. Physical Review B, 2019, 100, .</mml:math 	ni>xk‡mml	:mi <b>1</b> 3/mml:ms
71	High Anionic Conductive Form of PbxSn2–xF4. Chemistry of Materials, 2019, 31, 7704-7710.	3.2	11
72	Solar Water Oxidation by a Visible-Light-Responsive Tantalum/Nitrogen-Codoped Rutile Titania Anode	1.5	1

72 for Photoelectrochemical Water Splitting and Carbon Dioxide Fixation. ChemPhotoChem, 2019, 3, 3-3. 1.5

#	Article	IF	CITATIONS
73	Morphological Effect on Reaction Distribution Influenced by Binder Materials in Composite Electrodes for Sheet-type All-Solid-State Lithium-Ion Batteries with the Sulfide-based Solid Electrolyte. Journal of Physical Chemistry C, 2019, 123, 3292-3298.	1.5	53
74	Exothermal mechanisms in the charged LiNi1/3Mn1/3Co1/3O2 electrode layers for sulfide-based all-solid-state lithium batteries. Journal of Power Sources, 2019, 434, 226714.	4.0	29
75	Influence of microstructures on conductivity in Tysonite-type fluoride ion conductors. Solid State Ionics, 2019, 338, 113-120.	1.3	16
76	Oxygenâ€Ðoped Ta <sub>3</sub> N <sub>5</sub> Nanoparticles for Enhanced Z‣cheme Carbon Dioxide Reduction with a Binuclear Ruthenium(II) Complex under Visible Light. ChemPhotoChem, 2019, 3, 1027-1033.	1.5	10
77	Interfacial Stability of Phosphate-NASICON Solid Electrolytes in Ni-Rich NCM Cathode-Based Solid-State Batteries. ACS Applied Materials & Interfaces, 2019, 11, 23244-23253.	4.0	73
78	Operando Observation of Formation and Annihilation of Inhomogeneous Reaction Distribution in a Composite Electrode for Lithiumâ€ion Batteries. Batteries and Supercaps, 2019, 2, 688-694.	2.4	14
79	Electrochemical phase transformation accompanied with Mg extraction and insertion in a spinel MgMn <sub>2</sub> O <sub>4</sub> cathode material. Physical Chemistry Chemical Physics, 2019, 21, 23749-23757.	1.3	39
80	A Visible-Light-Driven Z-Scheme CO2 Reduction System Using Ta3N5 and a Ru(II) Binuclear Complex. Bulletin of the Chemical Society of Japan, 2019, 92, 124-126.	2.0	24
81	<i>In situ</i> Zn/ZnO mapping elucidating for "shape change―of zinc electrode. APL Materials, 2018, 6, .	2.2	17
82	Visible-light CO <sub>2</sub> reduction over a ruthenium( <scp>ii</scp> )-complex/C <sub>3</sub> N <sub>4</sub> hybrid photocatalyst: the promotional effect of silver species. Journal of Materials Chemistry A, 2018, 6, 9708-9715.	5.2	31
83	New Precursor Route Using a Compositionally Flexible Layered Oxide and Nanosheets for Improved Nitrogen Doping and Photocatalytic Activity. ACS Applied Energy Materials, 2018, 1, 1734-1741.	2.5	10
84	Grain-boundary-rich mesoporous NiTiO3 micro-prism as high tap-density, super rate and long life anode for sodium and lithium ion batteries. Energy Storage Materials, 2018, 13, 329-339.	9.5	40
85	Surface analysis of topmost layer of epitaxial layered oxide thin film: Application to delafossite oxide for oxygen evolution reaction. Surface Science, 2018, 668, 93-99.	0.8	7
86	Influence of TiO2 Support on Activity of Co3O4/TiO2 Photocatalysts for Visible-Light Water Oxidation. Bulletin of the Chemical Society of Japan, 2018, 91, 486-491.	2.0	16
87	Enhancement of Oxygen Reduction Reaction Activity of Pd Core-Pt Shell Structured Catalyst on a Potential Cycling Accelerated Durability Test. Electrocatalysis, 2018, 9, 125-138.	1.5	16
88	Effect of introducing interlayers into electrode/electrolyte interface in all-solid-state battery using sulfide electrolyte. Solid State Ionics, 2018, 327, 150-156.	1.3	38
89	High Rate Performance of Dual-Substituted LiFePO <sub>4</sub> Based on Controlling Metastable Intermediate Phase. ACS Applied Energy Materials, 2018, 1, 6736-6740.	2.5	9
90	Mechanistic Insight on the Formation of GaN:ZnO Solid Solution from Zn-Ga Layered Double Hydroxide Using Urea as the Nitriding Agent. Inorganic Chemistry, 2018, 57, 13953-13962.	1.9	20

#	Article	IF	CITATIONS
91	Dependency of the Charge–Discharge Rate on Lithium Reaction Distributions for a Commercial Lithium Coin Cell Visualized by Compton Scattering Imaging. Condensed Matter, 2018, 3, 27.	0.8	10
92	A Reversible Rocksalt to Amorphous Phase Transition Involving Anion Redox. Scientific Reports, 2018, 8, 15086.	1.6	21
93	Role of Coordination Structure of Magnesium Ions on Charge and Discharge Behavior of Magnesium Alloy Electrode. Journal of Physical Chemistry C, 2018, 122, 25204-25210.	1.5	30
94	Effects of Interfacial Electron Transfer in Metal Complex–Semiconductor Hybrid Photocatalysts on Z-Scheme CO <sub>2</sub> Reduction under Visible Light. ACS Catalysis, 2018, 8, 9744-9754.	5.5	60
95	Undoped Layered Perovskite Oxynitride Li <sub>2</sub> LaTa <sub>2</sub> O <sub>6</sub> N for Photocatalytic CO <sub>2</sub> Reduction with Visible Light. Angewandte Chemie, 2018, 130, 8286-8290.	1.6	17
96	Undoped Layered Perovskite Oxynitride Li <sub>2</sub> LaTa <sub>2</sub> O <sub>6</sub> N for Photocatalytic CO <sub>2</sub> Reduction with Visible Light. Angewandte Chemie - International Edition, 2018, 57, 8154-8158.	7.2	66
97	Site-Selective Analysis of Nickel-Substituted Li-Rich Layered Material: Migration and Role of Transition Metal at Charging and Discharging. Journal of Physical Chemistry C, 2018, 122, 20099-20107.	1.5	7
98	Investigation of charge compensation mechanism of LiNi <sub>â"</sub> Co <sub>â"</sub> Mn <sub>â"</sub> O <sub>2</sub> Positive Electrode during Initial Cha Process by <i>Operando</i> Soft X-ray XAFS Measurement. Journal of Surface Analysis (Online), 2018, 25, 90-102.	rge 0.1	3
99	Charge Compensation Mechanism in Li-Excess Oxides Revealed By Operando Soft/Hard X-Ray Absorption Spectroscopy. ECS Meeting Abstracts, 2018, , .	0.0	0
100	Visualization of Inhomogeneous Reaction Distribution in the Model LiCoO <sub>2</sub> Composite Electrode of Lithium Ion Batteries. Journal of Physical Chemistry C, 2017, 121, 2118-2124.	1.5	35
101	Hidden Two-Step Phase Transition and Competing Reaction Pathways in LiFePO <sub>4</sub> . Chemistry of Materials, 2017, 29, 2855-2863.	3.2	25
102	Direct observation of layered-to-spinel phase transformation in Li <sub>2</sub> MnO <sub>3</sub> and the spinel structure stabilised after the activation process. Journal of Materials Chemistry A, 2017, 5, 6695-6707.	5.2	72
103	Pressure-Stabilized Cubic Perovskite Oxyhydride BaScO <sub>2</sub> H. Inorganic Chemistry, 2017, 56, 4840-4845.	1.9	36
104	Structural and Electronic-State Changes of a Sulfide Solid Electrolyte during the Li Deinsertion–Insertion Processes. Chemistry of Materials, 2017, 29, 4768-4774.	3.2	151
105	Amorphous Metal Polysulfides: Electrode Materials with Unique Insertion/Extraction Reactions. Journal of the American Chemical Society, 2017, 139, 8796-8799.	6.6	84
106	Brownmilleriteâ€ŧype Ca <sub>2</sub> FeCoO <sub>5</sub> as a Practicable Oxygen Evolution Reaction Catalyst. ChemSusChem, 2017, 10, 2864-2868.	3.6	50
107	Charge–Discharge Behavior of Bismuth in a Liquid Electrolyte for Rechargeable Batteries Based on a Fluoride Shuttle. ACS Energy Letters, 2017, 2, 1460-1464.	8.8	77
108	Effect of Potential Profile on Battery Capacity Decrease during Continuous Cycling. Journal of Physical Chemistry C, 2017, 121, 6018-6023.	1.5	12

#	Article	IF	CITATIONS
109	Visualizing redox orbitals and their potentials in advanced lithium-ion battery materials using high-resolution x-ray Compton scattering. Science Advances, 2017, 3, e1700971.	4.7	24
110	Brownmillerite-type Ca2 FeCoO5 as a Practicable Oxygen Evolution Reaction Catalyst. ChemSusChem, 2017, 10, 2841-2841.	3.6	5
111	Effects of the SrTiO <sub>3</sub> support on visible-light water oxidation with Co <sub>3</sub> O <sub>4</sub> nanoparticles. Dalton Transactions, 2017, 46, 16959-16966.	1.6	10
112	<i>In operando</i> quantitation of Li concentration for a commercial Li-ion rechargeable battery using high-energy X-ray Compton scattering. Journal of Synchrotron Radiation, 2017, 24, 1006-1011.	1.0	17
113	Visualization of the reaction distribution in a composite cathode for an all-solid-state lithium-ion battery. Journal of the Ceramic Society of Japan, 2017, 125, 299-302.	0.5	13
114	Development of Li <sub>2</sub> TiS <sub>3</sub> –Li <sub>3</sub> NbS <sub>4</sub> by a mechanochemical process. Journal of the Ceramic Society of Japan, 2017, 125, 268-271.	0.5	11
115	æf屿™,代ã«ãŠã'ã,‹æ"⁻éf¨ã®å¼2¹å‰². Electrochemistry, 2017, 85, 383-383.	0.6	Ο
116	Electronic structure of oxide electrode materials studied by Compton profiles. Acta Crystallographica Section A: Foundations and Advances, 2017, 73, C1103-C1103.	0.0	0
117	Selective and low temperature transition metal intercalation in layered tellurides. Nature Communications, 2016, 7, 13809.	5.8	10
118	Structural and electronic features of binary Li2S-P2S5 glasses. Scientific Reports, 2016, 6, 21302.	1.6	100
119	Contactless analysis of electric dipoles at high- <i>k</i> /SiO2 interfaces by surface-charge-switched electron spectroscopy. Applied Physics Letters, 2016, 108, .	1.5	4
120	Discharge/charge reaction mechanisms of FeS2 cathode material for aluminum rechargeable batteries at 55°C. Journal of Power Sources, 2016, 313, 9-14.	4.0	137
121	Overpotential-Induced Introduction of Oxygen Vacancy in La <sub>0.67</sub> Sr <sub>0.33</sub> MnO <sub>3</sub> Surface and Its Impact on Oxygen Reduction Reaction Catalytic Activity in Alkaline Solution. Journal of Physical Chemistry C, 2016, 120, 6006-6010.	1.5	37
122	Structural Understanding of Superior Battery Properties of Partially Ni-Doped Li2MnO3 as Cathode Material. Journal of Physical Chemistry Letters, 2016, 7, 2063-2067.	2.1	29
123	Direct observation of reversible oxygen anion redox reaction in Li-rich manganese oxide, Li <sub>2</sub> MnO <sub>3</sub> , studied by soft X-ray absorption spectroscopy. Journal of Materials Chemistry A, 2016, 4, 9293-9302.	5.2	179
124	Anti-site mixing governs the electrochemical performances of olivine-type MgMnSiO <sub>4</sub> cathodes for rechargeable magnesium batteries. Physical Chemistry Chemical Physics, 2016, 18, 13524-13529.	1.3	39
125	Ligancy-Driven Controlling of Covalency and Metallicity in a Ruthenium Two-Dimensional System. Chemistry of Materials, 2016, 28, 5784-5790.	3.2	3
126	Dynamic Behavior at the Interface between Lithium Cobalt Oxide and an Organic Electrolyte Monitored by Neutron Reflectivity Measurements. Journal of Physical Chemistry C, 2016, 120, 20082-20088.	1.5	39

#	Article	IF	CITATIONS
127	Carbonaceous thin film coating with Fe–N 4 site for enhancement of dioxovanadium ion reduction. Journal of Power Sources, 2016, 324, 521-527.	4.0	7
128	Direct Synthesis of Carbon–Molybdenum Carbide Nanosheet Composites via a Pseudotopotactic Solid-State Reaction. Chemistry of Materials, 2016, 28, 8899-8904.	3.2	7
129	Quantitative Analysis of Transition-Metal Migration Induced Electrochemically in Lithium-Rich Layered Oxide Cathode and Its Contribution to Properties at High and Low Temperatures. Journal of Physical Chemistry C, 2016, 120, 27109-27116.	1.5	15
130	Real-time observations of lithium battery reactions—operando neutron diffraction analysis during practical operation. Scientific Reports, 2016, 6, 28843.	1.6	101
131	Ionic Conduction in Lithium Ion Battery Composite Electrode Governs Cross-sectional Reaction Distribution. Scientific Reports, 2016, 6, 26382.	1.6	123
132	Non-destructive measurement of <i>in-operando</i> lithium concentration in batteries via x-ray Compton scattering. Journal of Applied Physics, 2016, 119, .	1.1	31
133	Identifying a descriptor for <i>d</i> -orbital delocalization in cathodes of Li batteries based on x-ray Compton scattering. Applied Physics Letters, 2016, 109, .	1.5	20
134	Degradation analysis of 18650-type lithium-ion cells by operando neutron diffraction. Journal of Power Sources, 2016, 325, 404-409.	4.0	31
135	Platinum-Based Electrocatalysts for the Oxygen-Reduction Reaction: Determining the Role of Pure Electronic Charge Transfer in Electrocatalysis. ACS Catalysis, 2016, 6, 4195-4198.	5.5	35
136	Dependence of Structural Defects in Li <sub>2</sub> MnO <sub>3</sub> on Synthesis Temperature. Chemistry of Materials, 2016, 28, 4143-4150.	3.2	54
137	Lithium intercalation and structural changes at the LiCoO2 surface under high voltage battery operation. Journal of Power Sources, 2016, 307, 599-603.	4.0	37
138	Oxidation behaviour of lattice oxygen in Li-rich manganese-based layered oxide studied by hard X-ray photoelectron spectroscopy. Journal of Materials Chemistry A, 2016, 4, 5909-5916.	5.2	48
139	Communication—XAFS Analysis of Discharge/Charge Reactions on the Li/CuCl <sub>2</sub> Battery Cathode with LiPF <sub>6</sub> /Methyl Difluoroacetate Electrolyte. Journal of the Electrochemical Society, 2016, 163, A727-A729.	1.3	2
140	Irreversible phase transition between LiFePO4 and FePO4 during high-rate charge-discharge reaction by operando X-ray diffraction. Journal of Power Sources, 2016, 309, 122-126.	4.0	26
141	Structure analyses using X-ray photoelectron spectroscopy and X-ray absorption near edge structure for amorphous MS3 (M: Ti, Mo) electrodes in all-solid-state lithium batteries. Journal of Power Sources, 2016, 313, 104-111.	4.0	36
142	Elucidating the Driving Force of Relaxation of Reaction Distribution in LiCoO <sub>2</sub> and LiFePO <sub>4</sub> Electrodes Using X-ray Absorption Spectroscopy. Journal of Physical Chemistry C, 2016, 120, 4739-4743.	1.5	21
143	Phase transition kinetics of LiNi <sub>0.5</sub> Mn <sub>1.5</sub> O <sub>4</sub> analyzed by temperature-controlled operando X-ray absorption spectroscopy. Physical Chemistry Chemical Physics, 2016, 18, 1897-1904.	1.3	19
144	In-situ measurement of the lithium distribution in Li-ion batteries using micro-IBA techniques. Nuclear Instruments & Methods in Physics Research B, 2016, 371, 298-302.	0.6	17

#	Article	IF	CITATIONS
145	Factors determining the packing-limitation of active materials in the composite electrode of lithium-ion batteries. Journal of Power Sources, 2016, 301, 11-17.	4.0	65
146	Operando Soft X-Ray Absorption Study on Electronic Structure of Lithium-Rich Cathode Materials; Li2MnO3 and Li2RuO3. ECS Meeting Abstracts, 2016, , .	0.0	0
147	Operando Evaluation of Reaction Distribution in a Composite Electrode of Li-Ion Batteries By Using Two Dimensional X-Ray Absorption Spectroscopy. ECS Meeting Abstracts, 2016, , .	0.0	0
148	High-capacity Lithium-ion Storage System Using Unilamellar Crystallites of Exfoliated MoO2 Nanosheets. Chemistry Letters, 2015, 44, 1595-1597.	0.7	5
149	<i>Operando</i> X-ray Fluorescence Imaging for Zinc-based Secondary Batteries. Electrochemistry, 2015, 83, 849-851.	0.6	11
150	Solid Solution Domains at Phase Transition Front of Li <i><sub>x</sub></i> Ni <sub>0.5</sub> Mn <sub>1.5</sub> O <sub>4</sub> . Advanced Energy Materials, 2015, 5, 1500638.	10.2	31
151	Electronic, Structural, and Electrochemical Modulation of Electrostatic Self-Assembled 1T-MoS <sub>2 </sub> Nanosheets via Topotactic Structural Conversion. E-Journal of Surface Science and Nanotechnology, 2015, 13, 1-7.	0.1	0
152	Catalysis of Vanadium Ion Redox Reactions on Carbonaceous Material with Metal–N <sub>4</sub> Sites. ChemCatChem, 2015, 7, 2305-2308.	1.8	11
153	Delithiation/Lithiation Behavior of LiNi <sub>0.5</sub> Mn <sub>1.5</sub> O <sub>4</sub> Studied by In Situ and Ex Situ <sup>6,7</sup> Li NMR Spectroscopy. Journal of Physical Chemistry C, 2015, 119, 13472-13480.	1.5	32
154	7Li NMR Study on Irreversible Capacity of LiNi0.8-xCo0.15Al0.05MgxO2Electrode in a Lithium-Ion Battery. Journal of the Electrochemical Society, 2015, 162, A1315-A1318.	1.3	6
155	Compton scattering imaging of a working battery using synchrotron high-energy X-rays. Journal of Synchrotron Radiation, 2015, 22, 161-164.	1.0	23
156	Extracting the Redox Orbitals in Li Battery Materials with High-Resolution X-Ray Compton Scattering Spectroscopy. Physical Review Letters, 2015, 114, 087401.	2.9	41
157	Transformation of Leaf-like Zinc Dendrite in Oxidation and Reduction Cycle. Electrochimica Acta, 2015, 166, 82-87.	2.6	44
158	Effect of an Electrolyte Additive of Vinylene Carbonate on the Electronic Structure at the Surface of a Lithium Cobalt Oxide Electrode under Battery Operating Conditions. Journal of Physical Chemistry C, 2015, 119, 9791-9797.	1.5	55
159	Crystal Structural Changes and Charge Compensation Mechanism during Two Lithium Extraction/Insertion between Li <sub>2</sub> FeSiO <sub>4</sub> and FeSiO <sub>4</sub> . Journal of Physical Chemistry C, 2015, 119, 10206-10211.	1.5	52
160	Meso-scale characterization of lithium distribution in lithium-ion batteries using ion beam analysis techniques. Journal of Power Sources, 2015, 299, 587-595.	4.0	13
161	Dynamical Origin of Ionic Conductivity for Li <sub>7</sub> P <sub>3</sub> S <sub>11</sub> Metastable Crystal As Studied by <sup>6/7</sup> Li and <sup>31</sup> P Solid-State NMR. Journal of Physical Chemistry C, 2015, 119, 24248-24254.	1.5	47
162	Direct observation of reversible charge compensation by oxygen ion in Li-rich manganese layered oxide positive electrode material, Li1.16Ni0.15Co0.19Mn0.50O2. Journal of Power Sources, 2015, 276, 89-94.	4.0	136

#	Article	IF	CITATIONS
163	Structural modification by adding Li cations into Mg/Cs-TFSA molten salt facilitating Mg electrodeposition. RSC Advances, 2015, 5, 3063-3069.	1.7	3
164	Room-Temperature Electrodeposition of Mg Metal from Amide Salts Dissolved in Glyme-Ionic Liquid Mixture. Journal of the Electrochemical Society, 2014, 161, D102-D106.	1.3	45
165	Carbonaceous Hydrogenâ€Evolution Catalyst Containing Cobalt Surrounded by a Tuned Local Structure. ChemCatChem, 2014, 6, 2197-2200.	1.8	15
166	Novel spectro-electrochemical cell for <i>in situ</i> / <i>operando</i> observation of common composite electrode with liquid electrolyte by X-ray absorption spectroscopy in the tender X-ray region. Review of Scientific Instruments, 2014, 85, 084103.	0.6	29
167	Electrochemical Reactivity of Magnesium Ions with Sn-Based Binary Alloys (Cu-Sn, Pb-Sn, and In-Sn). ECS Transactions, 2014, 58, 75-80.	0.3	17
168	Origin of Surface Coating Effect for MgO on LiCoO <sub>2</sub> to Improve the Interfacial Reaction between Electrode and Electrolyte. Advanced Materials Interfaces, 2014, 1, 1400195.	1.9	56
169	Soft X-ray absorption spectroscopic studies with different probing depths: Effect of an electrolyte additive on electrode surfaces. Journal of Power Sources, 2014, 248, 994-999.	4.0	44
170	Evaluation of the effective reaction zone in a composite cathode for lithium ion batteries. Solid State lonics, 2014, 262, 66-69.	1.3	11
171	Characterization of Bulk and Surface Chemical States on Electrochemically Cycled LiFePO <sub>4</sub> : A Solid State NMR Study. Journal of the Electrochemical Society, 2014, 161, A1012-A1018.	1.3	10
172	Surface Strontium Segregation of Solid Oxide Fuel Cell Cathodes Proved by In Situ Depth-Resolved X-ray Absorption Spectroscopy. ECS Electrochemistry Letters, 2014, 3, F23-F26.	1.9	38
173	X-ray absorption fine structure imaging of inhomogeneous electrode reaction in LiFePO4 lithium-ion battery cathode. Journal of Power Sources, 2014, 269, 994-999.	4.0	55
174	First principles study of dopant solubility and defect chemistry in LiCoO <sub>2</sub> . Journal of Materials Chemistry A, 2014, 2, 11235-11245.	5.2	52
175	Kinetically asymmetric charge and discharge behavior of LiNi0.5Mn1.5O4 at low temperature observed by in situ X-ray diffraction. Journal of Materials Chemistry A, 2014, 2, 15414-15419.	5.2	12
176	Local Structure and Spin State of Cobalt Ion at Defect in Lithium Overstoichiometric LiCoO <sub>2</sub> As Studied by <sup>6/7</sup> Li Solid-State NMR Spectroscopy. Journal of Physical Chemistry C, 2014, 118, 15375-15385.	1.5	15
177	Spectroscopic X-ray Diffraction for Microfocus Inspection of Li-Ion Batteries. Journal of Physical Chemistry C, 2014, 118, 20750-20755.	1.5	31
178	Electrochemical and Spectroscopic Characterization of LiCoO <sub>2</sub> Thin-Film as Model Electrode. Journal of the Electrochemical Society, 2014, 161, A1447-A1452.	1.3	9
179	Relationship between Phase Transition Involving Cationic Exchange and Charge–Discharge Rate in Li2FeSiO4. Chemistry of Materials, 2014, 26, 1380-1384.	3.2	47
180	MgFePO <sub>4</sub> F as a feasible cathode material for magnesium batteries. Journal of Materials Chemistry A, 2014, 2, 11578-11582.	5.2	75

#	Article	IF	CITATIONS
181	Spontaneous Lithium Transportation via LiMn2O4/Electrolyte Interface Studied by 6/7Li Solid-State Nuclear Magnetic Resonance. Electrochimica Acta, 2014, 147, 540-544.	2.6	10
182	Improved Cyclic Performance of Lithium-Ion Batteries: An Investigation of Cathode/Electrolyte Interface via In Situ Total-Reflection Fluorescence X-ray Absorption Spectroscopy. Journal of Physical Chemistry C, 2014, 118, 9538-9543.	1.5	60
183	Local structural change in Li2FeSiO4 polyanion cathode material during initial cycling. Solid State Ionics, 2014, 262, 110-114.	1.3	11
184	High potential durability of LiNi0.5Mn1.5O4 electrodes studied byÂsurface sensitive X-ray absorption spectroscopy. Journal of Power Sources, 2014, 245, 816-821.	4.0	29
185	Pyrophosphate Na2FeP2O7 as a low-cost and high-performance positive electrode material for sodium secondary batteries utilizing an inorganic ionic liquid. Journal of Power Sources, 2014, 246, 783-787.	4.0	77
186	Relationship between Local Structure and Oxide Ionic Diffusion of Nd2NiO4+^ ^delta; with K2NiF4 Structure. Electrochemistry, 2014, 82, 875-879.	0.6	4
187	Stabilization of the Electronic Structure at the Cathode/Electrolyte Interface via MgO Ultra-thin Layer during Lithium-ions Insertion/Extraction. Electrochemistry, 2014, 82, 891-896.	0.6	21
188	Direct Observation of Rate Determining Step for Nd2NiO4+^ ^delta; SOFC Cathode Reaction by operando Electrochemical XAS. Electrochemistry, 2014, 82, 897-900.	0.6	12
189	Development of a new special environment powder neutron diffractomter, SPICA. Acta Crystallographica Section A: Foundations and Advances, 2014, 70, C1185-C1185.	0.0	0
190	New Magnesium-ion Conductive Electrolyte Solution Based on Triglyme for Reversible Magnesium Metal Deposition and Dissolution at Ambient Temperature. Chemistry Letters, 2014, 43, 1788-1790.	0.7	60
191	Development of SPICA, New Dedicated Neutron Powder Diffractometer for Battery Studies. Journal of Physics: Conference Series, 2014, 502, 012053.	0.3	43
192	Structural origin of ionic conductivity for Li <sub>7</sub> P <sub>3</sub> S <sub>11</sub> metastable crystal by neutron and X-ray diffraction. Journal of Physics: Conference Series, 2014, 502, 012021.	0.3	6
193	High energy density rechargeable magnesium battery using earth-abundant and non-toxic elements. Scientific Reports, 2014, 4, 5622.	1.6	286
194	RISING beamline (BL28XU) for rechargeable battery analysis. Journal of Synchrotron Radiation, 2014, 21, 268-272.	1.0	22
195	Layered Perovskite Oxide: A Reversible Air Electrode for Oxygen Evolution/Reduction in Rechargeable Metal-Air Batteries. Journal of the American Chemical Society, 2013, 135, 11125-11130.	6.6	194
196	Enhanced Anodic Dissolution of Magnesium in Quaternary-Ammonium-Based Ionic Liquid Containing a Small Amount of Water. Journal of the Electrochemical Society, 2013, 160, D453-D458.	1.3	12
197	A novel cationic-ordering fluoro-polyanionic cathode LiV0.5Fe0.5PO4F and its single phase Li+ insertion/extraction behaviour. RSC Advances, 2013, 3, 22935.	1.7	6
198	Phase Transition Analysis between LiFePO <sub>4</sub> and FePO <sub>4</sub> by In-Situ Time-Resolved X-ray Absorption and X-ray Diffraction. Journal of the Electrochemical Society, 2013, 160, A3061-A3065.	1.3	50

#	Article	IF	CITATIONS
199	Phase transition kinetics of LiNi0.5Mn1.5O4 electrodes studied by in situ X-ray absorption near-edge structure and X-ray diffraction analysis. Journal of Materials Chemistry A, 2013, 1, 10442.	5.2	56
200	Charge compensation mechanisms in Li1.16Ni0.15Co0.19Mn0.50O2 positive electrode material for Li-ion batteries analyzed by a combination of hard and soft X-ray absorption near edge structure. Journal of Power Sources, 2013, 222, 45-51.	4.0	130
201	Selective observation of a spinning-sideband manifold of paramagnetic solids by rotation-synchronized DANTE. Journal of Magnetic Resonance, 2013, 231, 66-71.	1.2	5
202	Visualization of conduction pathways in lithium superionic conductors: Li2S-P2S5 glasses and Li7P3S11 glass–ceramic. Chemical Physics Letters, 2013, 584, 113-118.	1.2	40
203	In situ NMR observation of the lithium extraction/insertion from LiCoO2 cathode. Electrochimica Acta, 2013, 108, 343-349.	2.6	51
204	Quantitating the Lattice Strain Dependence of Monolayer Pt Shell Activity toward Oxygen Reduction. Journal of the American Chemical Society, 2013, 135, 5938-5941.	6.6	112
205	High temperature defect chemistry in layered lithium transition-metal oxides based on first-principles calculations. Journal of Power Sources, 2013, 244, 592-596.	4.0	16
206	Direct Observation of a Metastable Crystal Phase of Li <sub><i>x</i></sub> FePO <sub>4</sub> under Electrochemical Phase Transition. Journal of the American Chemical Society, 2013, 135, 5497-5500.	6.6	177
207	Effects of ZrO <sub>2</sub> Coating on LiCoO <sub>2</sub> Thin-Film Electrode Studied by In Situ X-ray Absorption Spectroscopy. Journal of the Electrochemical Society, 2013, 160, A3054-A3060.	1.3	64
208	Transient Phase Change in Two Phase Reaction between LiFePO <sub>4</sub> and FePO <sub>4</sub> under Battery Operation. Chemistry of Materials, 2013, 25, 1032-1039.	3.2	122
209	In Situ Observation of Tin Negative Electrode / Electrolyte Interface by X-ray Reflectivity. ECS Transactions, 2013, 50, 31-37.	0.3	4
210	In situ two-dimensional micro-imaging XAFS with CCD detector. Journal of Physics: Conference Series, 2013, 430, 012021.	0.3	5
211	<i>in situ</i> Analysis Technique for Development of High-Energy Density Battery of Electric Vehicle. Journal of the Institute of Electrical Engineers of Japan, 2013, 133, 153-156.	0.0	0
212	Average and Local Structure Analyses of Li(Mn <sub>1/3</sub> Ni <sub>1/3</sub> Co <sub>1/3â^'x</sub> Al <sub>x</sub> )O <sub>2</sub> Using Neutron and Synchrotron X-ray Sources. Journal of the Electrochemical Society, 2012, 159, A673-A677.	1.3	13
213	1.Xç·šå¸åŽå^†å‰æ³•ã«ã,^ã,<リãƒã,¦ãƒã,≋ン二æ¬jé›»æ±é›»æ¥µãƒ»é›»è§£è³ªç•Œé¢ã«ãŠãʿã,‹in situæ,¬ Co <mml:math <="" td="" xmlns:mml="http://www.w3.org/1998/Math/MathML"><td>å®<b>ĕ.</b>Ælectr</td><td>ochemistry,</td></mml:math>	å® <b>ĕ.</b> Ælectr	ochemistry,
214	display="inline"> <mml:mi>K</mml:mi> -edge XANES of LiCoO <mml:math xmlns:mml="http://www.w3.org/1998/Math/MathML" display="inline"&gt;<mml:msub><mml:mrow /&gt;<mml:mn>2</mml:mn></mml:mrow </mml:msub>and CoO<mml:math xmlns:mml="http://www.w3.org/1998/Math/Math/ML" display="inline"&gt;<mml:msub><mml:mrow< td=""><td>1.1</td><td>23</td></mml:mrow<></mml:msub></mml:math </mml:math 	1.1	23
215	/> <mml:mn>2</mml:mn> with a variety of structures by supercell density fun Filst Inâ€Situ Observation of the LiCoO <sub>2</sub> Electrode/Electrolyte Interface by Totalâ€Reflection Xâ€ray Absorption Spectroscopy. Angewandte Chemie - International Edition, 2012, 51, 11597-11601.	7.2	167
	Defect Chemistry in Layered Lici>Mc/i>Ocsub>2c/sub> (ci>Mc/i> = Co. Ni. Mn. and) Ti FTOo0.0.0 rgBT /Overloc	b 10 Tf 50	67 Td (Lize

216

Defect Chemistry in Layered Li<i>M</i>O<sub>2</sub> (<i>M</i> = Co, Ni, Mn, and) Tj ETQq0 0 0 rgBT /Overlock 10 Tf 50 67 Td (Li<sub 3.2 128 3886-3894.

#	Article	IF	CITATIONS
217	Association of paramagnetic species with formation of LiF at the surface of LiCoO2. Electrochimica Acta, 2012, 78, 49-54.	2.6	22
218	Electrochemical characterization of single-layer MnO2 nanosheets as a high-capacitance pseudocapacitor electrode. Journal of Materials Chemistry, 2012, 22, 14691.	6.7	48
219	Anodic Dissolution Behavior of Magnesium in Hydrophobic Ionic Liquids. ECS Transactions, 2011, 33, 65-70.	0.3	4
220	An X-ray absorption spectroscopic study on mixed conductive La0.6Sr0.4Co0.8Fe0.2O3â~δ cathodes. I. Electrical conductivity and electronic structure. Physical Chemistry Chemical Physics, 2011, 13, 16637.	1.3	34
221	Local structural analysis for oxide ion transport in La0.6Sr0.4FeO3â~î´ cathodes. Journal of Materials Chemistry, 2011, 21, 14013.	6.7	15
222	Role of Local and Electronic Structural Changes with Partially Anion substitution Lithium Manganese Spinel Oxides on Their Electrochemical Properties: X-ray Absorption Spectroscopy Study. Dalton Transactions, 2011, 40, 9752.	1.6	26
223	Pore Development in Carbonized Hemoglobin by Concurrently Generated MgO Template for Activity Enhancement as Fuel Cell Cathode Catalyst. ACS Applied Materials & Interfaces, 2011, 3, 4837-4843.	4.0	18
224	Theoretical Fingerprints of Transition Metal L <sub>2,3</sub> XANES and ELNES for Lithium Transition Metal Oxides by ab Initio Multiplet Calculations. Journal of Physical Chemistry C, 2011, 115, 11871-11879.	1.5	34
225	X-ray Absorption Spectroscopic Study on La <sub>0.6</sub> Sr <sub>0.4</sub> CoO <sub>3â^îî</sub> Cathode Materials Related with Oxygen Vacancy Formation. Journal of Physical Chemistry C, 2011, 115, 16433-16438.	1.5	56
226	Nanosized Effect on Electronic/Local Structures and Specific Lithium-Ion Insertion Property in TiO <sub>2</sub> –B Nanowires Analyzed by X-ray Absorption Spectroscopy. Chemistry of Materials, 2011, 23, 3636-3644.	3.2	30
227	Lithium-Ion Transfer Reaction at the Interface between Partially Fluorinated Insertion Electrodes and Electrolyte Solutions. Journal of Physical Chemistry C, 2011, 115, 12990-12994.	1.5	23
228	Effect of average and local structures on lithium ion conductivity in La2/3â^'xLi3xTiO3. Journal of Materials Chemistry, 2011, 21, 10195.	6.7	25
229	Depth-resolved X-ray absorption spectroscopic study on nanoscale observation of the electrode–solid electrolyte interface for all solid state lithium ion batteries. Journal of Materials Chemistry, 2011, 21, 10051.	6.7	93
230	Nanoscale Observation of the Electronic and Local Structures of LiCoO <sub>2</sub> Thin Film Electrode by Depth-Resolved X-ray Absorption Spectroscopy. Journal of Physical Chemistry Letters, 2011, 2, 2511-2514.	2.1	50
231	Improvement of lithium ion conductivity for A-site disordered lithium lanthanum titanate perovskite oxides by fluoride ion substitution. Journal of Materials Chemistry, 2011, 21, 10061.	6.7	14
232	Electronic and local structural changes with lithium-ion insertion in TiO2-B: X-ray absorption spectroscopy study. Journal of Materials Chemistry, 2011, 21, 15369.	6.7	49
233	Direct Evidence of LiF Formation at Electrode/Electrolyte Interface by 7Li and 19F Double-Resonance Solid-State NMR Spectroscopy. Electrochemical and Solid-State Letters, 2011, 14, A134.	2.2	28
234	In situ æ,¬å®šï¼^5)Xç·šååŽå^†å‰æ³• 蓄電æ±Â·SOFC. Electrochemistry, 2011, 79, 720-727.	0.6	0

#	Article	IF	CITATIONS
235	Dependence of Thermodynamic Stability, Crystal and Electronic Structures and Battery Characteristic on Synthetic Condition and Li Content for LixMn0.5Ni0.5O2 as a Cathode Active Material of Li-Ion Battery. Electrochemistry, 2011, 79, 15-23.	0.6	4
236	Thickness estimation of interface films formed on Li1â^'xCoO2 electrodes by hard X-ray photoelectron spectroscopy. Journal of Power Sources, 2011, 196, 10679-10685.	4.0	29
237	Dependence of property, cathode characteristics, thermodynamic stability, and average and local structures on heat-treatment condition for LiNi0.5Mn0.5O2 as a cathode active material for Li-ion battery. Electrochimica Acta, 2011, 56, 9453-9458.	2.6	10
238	<i>In situ</i> two-dimensional imaging quick-scanning XAFS with pixel array detector. Journal of Synchrotron Radiation, 2011, 18, 919-922.	1.0	18
239	Effect of cation doping on ionic and electronic properties for lanthanum silicate-based solid electrolytes. Solid State Ionics, 2011, 192, 195-199.	1.3	22
240	Nanoprotonics in perovsikte-type oxides: Reversible changes in color and ion conductivity due to nanoionics phenomenon in platinum-containing perovskite oxide. Solid State Ionics, 2011, 182, 13-18.	1.3	16
241	Performance of Fe-Co-Ni/C Anode Catalyst on Direct Ethanol Fuel Cell. ECS Transactions, 2011, 41, 2205-2209.	0.3	4
242	Lithium-Ion Conductivity in Lithium Lanthanum Titanates as Different Local Distortion Model Compounds. Electrochemistry, 2010, 78, 457-459.	0.6	0
243	Electrochemical Behavior of Platinum Electrode in 2-Methyltetrahydrofuran Containing Magnesium Bromide. ECS Meeting Abstracts, 2010, MA2010-02, 52-52.	0.0	5
244	Nonprecious Metal Electrocatalysts for Alkaline Fuel Cells. ECS Transactions, 2010, 28, 153-158.	0.3	3
245	Ionic and Electronic Conductivities and Fuel Cell Performance of Oxygen Excess-Type Lanthanum Silicates. Journal of the Electrochemical Society, 2010, 157, B1465.	1.3	23
246	Effect of Reduction Temperature of Fe-Co-Ni/C Catalyst on the Solid Alkaline Fuel Cell Performance. ECS Transactions, 2010, 33, 1817-1821.	0.3	0
247	New Oxygen Reduction Electrocatalysts Based on Oxide Nanosheet Materials. ECS Transactions, 2009, 16, 97-105.	0.3	2
248	Investigation on Oxygen Potential Distribution in a ZrO <sub>2</sub> -Based Solid Electrolyte by Using In-Situ Micro XAS Technique. ECS Transactions, 2009, 25, 345-348.	0.3	2
249	Determination of lithium ion diffusion in lithium–manganese-oxide-spinel thin films by secondary-ion mass spectrometry. Journal of Power Sources, 2009, 189, 643-645.	4.0	24
250	Improvement of Li-ion conductivity in A-site disordering lithium-lanthanum-titanate perovskite oxides by adding LiF in synthesis. Journal of Power Sources, 2009, 189, 536-538.	4.0	23
251	Electrocatalytic Activity of the Pyrochlores Ln2M2O7â <sup>~</sup> δ (LnÂ=ÂLanthanoids) for Oxygen Reduction Reaction. Topics in Catalysis, 2009, 52, 896-902.	1.3	10
252	Oxygen Reduction Electrode Properties of Manganese Oxide Nanosheet-Based Materials. Topics in Catalysis, 2009, 52, 903-911.	1.3	12

#	Article	IF	CITATIONS
253	Electronic structures of partially fluorinated lithium manganese spinel oxides and their electrochemical properties. Journal of Power Sources, 2009, 189, 599-601.	4.0	11
254	Cathode having high rate performance for a secondary Li-ion cell surface-modified by aluminum oxide nanoparticles. Journal of Power Sources, 2009, 189, 471-475.	4.0	11
255	Visualization of oxygen transport behavior at metal electrode/oxide electrolyte interface using secondary ion mass spectrometry. Solid State Ionics, 2008, 179, 347-354.	1.3	20
256	Anomalous transport property at surface and interface of metal/rare earth doped ceria. Solid State Ionics, 2008, 179, 1343-1346.	1.3	9
257	Oxygen nonstoichiometry of the perovskite-type oxides BaCe0.9M0.1O3â^' (M Y, Yb, Sm, Tb, and Nd). Solid State Ionics, 2008, 179, 529-535.	1.3	40
258	Hemoglobin Pyropolymer Used as a Precursor of a Noble-Metal-Free Fuel Cell Cathode Catalyst. Journal of Physical Chemistry C, 2008, 112, 2784-2790.	1.5	55
259	X-Ray Absorption Spectroscopic Studies on Electronic Structure in La <sub>0.6</sub> Sr <sub>0.4</sub> Co <sub>0.8</sub> Fe <sub>0.2</sub> O <sub>3-δ</sub> Perovskite-Type Oxides. ECS Transactions, 2008, 13, 201-205.	0.3	3
260	Studies on Defect Structures of (La,Sr)2NiO4 by Using X-ray Absorption Spectroscopy. ECS Transactions, 2008, 13, 195-200.	0.3	0
261	Electronic and Local Structures of La1-x SrxCoO3-δ Studied by In-Situ Micro XAS Measurements. ECS Transactions, 2008, 13, 161-164.	0.3	3
262	Electrocatalytic O2 Reduction Properties of Pyrochlore-Type Oxides for Alkaline DAFCs. ECS Transactions, 2008, 16, 891-900.	0.3	4
263	XAS Study for Degradation Mechanism of Pt/C Catalyst During Potential Cycling Test. ECS Transactions, 2007, 11, 1321-1329.	0.3	15
264	A Model Study for Oxygen Reduction Reaction and Durability of Pt/C Catalyst in Triple-Phase Boundary of PEFCs. ECS Transactions, 2007, 11, 809-818.	0.3	6
265	Meniscus Formation and Hydrogen Oxidation on Partially Immersed Pt-Carbon Electrode. Electrochemistry, 2007, 75, 248-257.	0.6	2
266	Scientific Aspects of Polymer Electrolyte Fuel Cell Durability and Degradation. Chemical Reviews, 2007, 107, 3904-3951.	23.0	2,976
267	Changes in Electronic Structure upon Lithium Insertion into Fe2(SO4)3and Fe2(MoO4)3Investigated by X-ray Absorption Spectroscopy. Journal of Physical Chemistry B, 2007, 111, 1424-1430.	1.2	40
268	Morphologic and crystallographic studies on electrochemically formed chromium nitride films. Electrochimica Acta, 2007, 53, 122-126.	2.6	1
269	Electrical conduction properties of Sr-doped Bi4(SiO4)3 with the eulytite-type structure. Journal of Materials Science, 2007, 42, 6566-6571.	1.7	6
270	Electrochemical effect of gold nanoparticles on Pt/α-Fe2O3/C for use in methanol oxidation in alkaline solution. Electrochimica Acta, 2007, 52, 3582-3587.	2.6	13

#	Article	IF	CITATIONS
271	Synthesis and Structural Study on MnO2Nanosheet Material by X-ray Absorption Spectroscopic Technique. Journal of Physical Chemistry B, 2006, 110, 174-177.	1.2	36
272	Electronic and local structural changes in Li2+xTi3O7ramsdellite compounds upon electrochemical Li-ion insertion reactions by X-ray absorption spectroscopy. Physical Chemistry Chemical Physics, 2006, 8, 882-889.	1.3	20
273	High CO Tolerance ofN,N-Ethylenebis(salicylideneaminato)oxovanadium(IV) as a Cocatalyst to Pt for the Anode of Reformate Fuel Cells. Chemistry of Materials, 2006, 18, 4505-4512.	3.2	14
274	Changes in Electronic Structure upon Li Insertion Reaction of Monoclinic Li3Fe2(PO4)3. Journal of Physical Chemistry B, 2006, 110, 17743-17750.	1.2	23
275	会誌"Electrochemistryâ€èªŒã,'ã,^ã,Šæ´»ç‴ã⊷ã┥é,ããŸã,ã«. Electrochemistry, 2006, 74, 803.	0.6	Ο
276	Application of SIMS analyses on oxygen transport in SOFC materials. Applied Surface Science, 2006, 252, 7045-7047.	3.1	8
277	High temperature protonic conduction in Sr-doped LaP3O9. Solid State Ionics, 2006, 177, 2407-2411.	1.3	25
278	Electrical conduction properties of rare earth orthophosphates under reducing conditions. Solid State Ionics, 2006, 177, 2369-2373.	1.3	10
279	Active parts for CH4 decomposition and electrochemical oxidation at metal/oxide interfaces by isotope labeling-secondary ion mass spectrometry. Solid State Ionics, 2006, 177, 3179-3185.	1.3	17
280	Oxygen nonstoichiometry, mixed valency and mixed conduction in (La,Sr)(Co,Fe)O3â <sup>~1</sup> Î. Solid State Ionics, 2006, 177, 1803-1806.	1.3	21
281	Influence of ligand structures on methanol electro-oxidation by mixed catalysts based on platinum and organic metal complexes for DMFC. Journal of Molecular Catalysis A, 2006, 248, 99-108.	4.8	10
282	Site-Directed Solid-State NMR on Membrane Proteins. Annual Reports on NMR Spectroscopy, 2006, 57, 99-175.	0.7	12
283	Multiple Scattering Calculation for Co K-Edge XANES Spectra of Nanometer-Scale Metal Deposited during Li Insertion into LiCoVO[sub 4]. Electrochemical and Solid-State Letters, 2006, 9, A200.	2.2	10
284	Investigation on cyclability in LixLa1/3NbO3 electrode material for rechargeable lithium ion battery. Journal of Power Sources, 2005, 146, 674-677.	4.0	6
285	Charge-transfer reaction rate at the LiMn2O4 spinel oxide cathode/polymer electrolyte interface. Solid State Ionics, 2005, 176, 2377-2381.	1.3	12
286	Electrochemical Performance of Lithium Polymer Battery Based on PC/Polymer Borate Ester Plasticizers. Electrochemical and Solid-State Letters, 2005, 8, A30.	2.2	5
287	High-Rate-Capable Lithium-Ion Battery Based on Surface-Modified Natural Graphite Anode and Substituted Spinel Cathode for Hybrid Electric Vehicles. Journal of the Electrochemical Society, 2005, 152, A1595.	1.3	33
288	Changes in Electronic Structure upon Lithium Insertion into the A-Site Deficient Perovskite Type Oxides (Li,La)TiO3. Journal of Physical Chemistry B, 2005, 109, 4135-4143.	1.2	67

#	Article	IF	CITATIONS
289	Experimental and Computational Study of the Electronic Structural Changes in LiTi2O4Spinel Compounds upon Electrochemical Li Insertion Reactions. Journal of Physical Chemistry B, 2005, 109, 1130-1134.	1.2	41
290	Lithium Ion Phase-Transfer Reaction at the Interface between the Lithium Manganese Oxide Electrode and the Nonaqueous Electrolyte. Journal of Physical Chemistry B, 2005, 109, 13322-13326.	1.2	54
291	X-ray Absorption Spectroscopic Study on the Electronic Structure of Li1-xCoPO4Electrodes as 4.8 V Positive Electrodes for Rechargeable Lithium Ion Batteries. Journal of Physical Chemistry B, 2005, 109, 11197-11203.	1.2	37
292	X-ray absorption study of the electronic structure of Li-excess spinel Li1+xTi2â^'xO4 (0⩽x⩽0.33). Appli Physics Letters, 2004, 84, 4364-4366.	ed 1.5	13
293	Relationship between the Li ionic conduction and the local structures in LiyLa(1â^'y)/3NbO3. Applied Physics Letters, 2004, 84, 4227-4229.	1.5	14
294	Soft Xâ€ray Absorption Near Edge Structure Analysis on Lithium Manganese Oxide Prepared by Microwave Heating. Journal of the American Ceramic Society, 2004, 87, 1002-1007.	1.9	11
295	Changes in Electronic Structure between Cobalt and Oxide Ions of Lithium Cobalt Phosphate as 4.8-V Positive Electrode Material. Chemistry of Materials, 2004, 16, 3399-3401.	3.2	80
296	A High Electrode-Reaction Rate for High-Power-Density Lithium-Ion Secondary Batteries by the Addition of a Lewis Acid. Angewandte Chemie - International Edition, 2004, 43, 1966-1969.	7.2	19
297	Ionic conductivity and transport number of lithium ion in polymer electrolytes containing PEG–borate ester. Electrochimica Acta, 2004, 50, 281-284.	2.6	39
298	Li2NiTiO4?a new positive electrode for lithium batteries: soft-chemistry synthesis and electrochemical characterization. Solid State Ionics, 2004, 172, 39-45.	1.3	43
299	Changes in electronic structure upon lithium insertion reaction into the A-site-deficient perovskite-type oxides, Gd1/3TaO3Part 1. XAS measurements. Solid State Ionics, 2004, 172, 73-76.	1.3	8
300	Lewis acidity and hardness of group 13/III metal centered alkoxides and their effects on ionic conductivity of polymer electrolytes. Solid State Ionics, 2004, 172, 63-67.	1.3	3
301	Changes in electronic structure upon lithium insertion reaction into the A-site deficient perovskite type oxides, Gd1/3TaO3Part 2. Ab initio calculation. Solid State Ionics, 2004, 172, 77-80.	1.3	3
302	Lithium Insertion/Removal Mechanism of LiCoVO[sub 4] in Lithium-Ion Cells. Electrochemical and Solid-State Letters, 2004, 7, A27.	2.2	13
303	XANES and EXAFS analysis of nano-size manganese dioxide as a cathode material for lithium-ion batteriesElectronic supplementary information (ESI) available: raw XAFS data; imaginary part of the FT; inverse FT. See http://www.rsc.org/suppdata/jm/b3/b315443b/. Journal of Materials Chemistry, 2004, 14, 1843.	6.7	51
304	Charge-Transfer Reaction Rate of Li+/Li Couple in Poly(ethylene glycol) Dimethyl Ether Based Electrolytes. Journal of Physical Chemistry B, 2004, 108, 4794-4798.	1.2	24
305	Molecular Dynamics Simulations of LiCoyMn2-yO4Cathode Materials for Rechargeable Li Ion Batteries. Journal of Physical Chemistry B, 2004, 108, 3754-3759.	1.2	18
306	Preparation of cathode active materials for lithium ion secondary batteries utilizing microwave irradiation: Part II. Electronic structure of lithium manganese oxide. Journal of Materials Research, 2004, 19, 2421-2427.	1.2	3

#	Article	IF	CITATIONS
307	XAFS Study of Reaction Mechanism of Nano-sized Manganese Dioxide as Cathode Materials for Lithium-ion Batteries. Electrochemistry, 2004, 72, 395-398.	0.6	2
308	Grain size control of LiMn2O4 cathode material using microwave synthesis method. Solid State lonics, 2003, 164, 35-42.	1.3	80
309	Local Structural Studies of LiCryMn2-yO4Cathode Materials for Li-Ion Batteries. Journal of Physical Chemistry B, 2003, 107, 1727-1733.	1.2	29
310	Interaction between the Lewis Acid Group of a Borate Ester and Various Anion Species in a Polymer Electrolyte Containing Mg Salt. Journal of Physical Chemistry B, 2003, 107, 11608-11614.	1.2	34
311	Using X-ray Absorption Spectroscopy to Measure Changes of Electronic Structure Accompanying Lithium Insertion into the Perovskite Type Oxides. Chemistry of Materials, 2003, 15, 1728-1733.	3.2	24
312	Changes in Local Structure during Electrochemical Li Insertion into A-Site Deficient Perovskite Oxides, La1/3NbO3. Journal of Physical Chemistry B, 2003, 107, 10715-10721.	1.2	22
313	Study on the AC Impedance Spectroscopy for the Li Insertion Reaction of LixLa1/3NbO3at the Electrodeâ^'Electrolyte Interface. Journal of Physical Chemistry B, 2003, 107, 10603-10607.	1.2	77
314	Influence of Lewis acidic borate ester groups on lithium ionic conduction in polymer electrolytes. Journal of Materials Chemistry, 2003, 13, 280-285.	6.7	34
315	Charge–discharge reaction mechanism of manganese molybdenum vanadium oxide as a high capacity anode material for Li secondary battery. Journal of Materials Chemistry, 2003, 13, 897-903.	6.7	22
316	Influence of PEG-Borate Ester as a Lewis Acid on Ionic Conductivity of Polymer Electrolyte Containing Mg-Salt. Journal of the Electrochemical Society, 2003, 150, A477.	1.3	28
317	First Principles Calculations of Formation Energies and Electronic Structures of Defects in Oxygen-Deficient LiMn[sub 2]O[sub 4]. Journal of the Electrochemical Society, 2003, 150, A63.	1.3	40
318	Preparation and Electrochemical Properties of Stoichiometric and Nonstoichiometric LiCo[sub x]Mn[sub 2â^'x]O[sub 4â^'Î]. Journal of the Electrochemical Society, 2003, 150, A1250.	1.3	27
319	Investigation of the Effect of Lewis Acid on Ionic Conductivity of Polymer Electrolyte Containing Mg Salt. Journal of the Electrochemical Society, 2003, 150, A726.	1.3	21
320	Preparation of Novel Solid Polymer Electrolytes Containing Group 13/III Metal Alkoxides as Lewis Acid. Electrochemistry, 2003, 71, 1028-1029.	0.6	1
321	O K-edge X-ray Absorption Spectroscopic Studies of Li <i><sub>x</sub></i> La <sub>1/3</sub> NbO <sub>3</sub> using <i>ab initio</i> Multiple Scattering Calculation. Electrochemistry, 2003, 71, 1025-1027.	0.6	3
322	Relationship between the Li ionic conduction and the local structures in B-site substituted perovskite compounds, (Li0.1La0.3)1+xMxNb1â^'xO3 (M=Zr, Ti; x=0, 0.05). Applied Physics Letters, 2002, 81, 2977-2979.	1.5	10
323	Influence of oxygen stoichiometry on the spin-glass behavior ofLiCrMnO4â <sup>~</sup> δspinels. Physical Review B, 2002, 66, .	1.1	11
324	Enhancement of Rate Capability in Graphite Anode by Surface Modification with Zirconia. Electrochemical and Solid-State Letters, 2002, 5, A275.	2.2	72

#	Article	IF	CITATIONS
325	Electrochemical Lithium Insertion for Perovskite Oxides of LiyLa(1-y)/3NbO3 (y = 0, 0.1, 0.25). Physical Chemistry B, 2002, 106, 6437-6441.	Journal of	33
326	lonic conduction of lithium in B-site substituted perovskite compounds, (Li0.1La0.3)yMxNb1 – xO3 (M =) Tj ET	Qq0,0 0 rg 6.7	BT_Overlocl
327	Charge–discharge reaction mechanism of manganese vanadium oxide as a high capacity anode material for lithium secondary battery. Journal of Materials Chemistry, 2002, 12, 3717-3722.	6.7	51
328	Electrochemical properties of manganese vanadium molybdenum oxide as the anode for Li secondary batteries. Journal of Materials Chemistry, 2002, 12, 2507-2512.	6.7	35
329	Crystal Structure Control of Lithium Manganese Spinel Oxides and Their Application to Lithium Secondary Battery. Nippon Kagaku Kaishi / Chemical Society of Japan - Chemistry and Industrial Chemistry Journal, 2002, 2002, 271-280.	0.1	1
330	Structural stability in partially substituted lithium manganese spinel oxide cathode. Ionics, 2002, 8, 329-338.	1.2	14
331	Reaction mechanisms of MnMoO4 for high capacity anode material of Li secondary battery. Solid State lonics, 2002, 146, 249-256.	1.3	106
332	Thermally stable solid polymer electrolyte containing borate ester groups for lithium secondary battery. Solid State Ionics, 2002, 152-153, 155-159.	1.3	19
333	Polymer electrolyte plasticized with PEG-borate ester having high ionic conductivity and thermal stability. Solid State Ionics, 2002, 150, 355-361.	1.3	89
334	Influence of PEG-borate ester on thermal property and ionic conductivity of the polymer electrolyte. Magyar Apróvad Közlemények, 2002, 69, 889-896.	1.4	11
335	Molecular dynamics study on lattice defects and heat capacity of LiCr1/6Mn11/6O4-d. Magyar Apróvad Közlemények, 2002, 69, 997-1004.	1.4	2
336	Enhancement of Electrochemical Reaction Rate by Deposition of Alumina on Natural Graphite Surface. Electrochemistry, 2001, 69, 830-833.	0.6	7
337	Changes in electronic structure by Li ion deintercalation in LiNiO2 from nickel L-edge and O K-edge XANES. Journal of Power Sources, 2001, 97-98, 326-327.	4.0	67
338	Changes in electronic structure by Li ion deintercalation in LiCoO2from cobaltL-edge and oxygenK-edge XANES. Journal of Synchrotron Radiation, 2001, 8, 872-873.	1.0	33
339	EXAFS study of crystal structures of (Ba1â^'xLax)2In2O5+xand their oxide ion conductivity. Journal of Synchrotron Radiation, 2001, 8, 857-859.	1.0	15
340	Thermally stable polymer electrolyte plasticized with PEG-borate ester for lithium secondary battery. Electrochemistry Communications, 2001, 3, 128-130.	2.3	51
341	Electrochemical Performance of Natural Graphite by Surface Modification Using Aluminum. Electrochemical and Solid-State Letters, 2001, 4, A109.	2.2	87
342	Micro Pattern of TiO <sub>2</sub> Thin Film Formation by Direct Synthesis From Aqueous Solution and Transcription of Resist Pattern. Materials Research Society Symposia Proceedings, 2000, 623, 423.	0.1	2

#	Article	IF	CITATIONS
343	Crystal structure of Ga-doped Ba2In2O5 and its oxide ion conductivity. Solid State Ionics, 2000, 132, 189-198.	1.3	88
344	Synthesis of (La,Sr)MeO3 (Me=Cr, Mn, Fe, Co) solid solutions from aqueous solutions. Solid State Ionics, 2000, 135, 359-364.	1.3	12
345	Reactions in Vaporâ€Phase Electrolytic Deposition for Preparing Yttriaâ€Stabilized Zirconia Thin Films. Journal of the American Ceramic Society, 2000, 83, 77-81.	1.9	10
346	Preparation of Thin Cation-Exchange Membranes Using Glow Discharge Plasma Polymerization and Its Reactions. Journal of the Electrochemical Society, 2000, 147, 111.	1.3	18
347	Crystal Structure of (Ba <sub>1-</sub> <i><sub>x</sub></i> La <i><sub>x</sub></i> ) <sub>2</sub> In <sub>2</sub> O <sub>5+</sub> <td>i<b>∞e</b>ub&gt;x</td> <td><!--886--></td>	i <b>∞e</b> ub>x	886
348	EXAFS Study of Coordination Structures of Gd-doped Ba2In2O5. Japanese Journal of Applied Physics, 1999, 38, 111.	0.8	10
349	Preparation of Perovskiteâ€Type La1 â~' x Sr x MnO3 Films by Vaporâ€Phase Processes and Their Electrochemical Properties: II. Effects of Doping Strontium to on the Electrode Properties. Journal of the Electrochemical Society, 1998, 145, 1999-2004.	1.3	42
350	Kinetics of Vaporâ€Phase Electrolytic Deposition of Yttriaâ€Stabilized Zirconia Thin Films. Journal of the Electrochemical Society, 1998, 145, 4277-4281.	1.3	2
351	Preparation of Perovskiteâ€Type La1 â~' x Sr x MnO3 Films by Vaporâ€Phase Processes and Their Electrochemical Properties. Journal of the Electrochemical Society, 1997, 144, 1362-1370.	1.3	38
352	Preparation and Characteristics of LaMnO3Thin Film Electrode on YSZ by a Vapor-Phase Process. Chemistry Letters, 1996, 25, 949-950.	0.7	0
353	Preparation of functionally gradient fluorocarbon polymer films by plasma polymerization of NF3 and propylene. Journal of Polymer Science Part A, 1996, 34, 193-198.	2.5	9
354	Preparation and Characteristics of Ni/YSZ Cermet Anodes by Vapor-phase Deposition. Electrochemistry, 1996, 64, 562-567.	0.3	9
355	Electrochemistry using plasma. Advanced Materials, 1995, 7, 323-325.	11.1	24
356	Novel Method for Preparing Nickel/YSZ Cermet by a Vapor-Phase Process. Journal of the American Ceramic Society, 1995, 78, 593-598.	1.9	28
357	Enhancement of the monovalent cation perm-selectivity of Nafion by plasma-induced surface modification. Journal of Adhesion Science and Technology, 1995, 9, 615-625.	1.4	8
358	Preparation of Thin Perfluorosulfonate Cationâ€Exchanger Films by Plasma Polymerization. Journal of the Electrochemical Society, 1994, 141, 2350-2355.	1.3	36
359	Vapour phase electrolytic deposition: a novel method for preparation of orientated thin films. Journal of the Chemical Society Chemical Communications, 1994, , 585.	2.0	5
360	Polymerizationâ€pressure dependencies of properties of perfluorosulfonate cationâ€exchanger thin films by plasma polymerization. Zeitschrift Fur Elektrotechnik Und Elektrochemie, 1994, 98, 631-635.	0.9	14

#	Article	IF	CITATIONS
361	Modification of lithium/electrolyte interface by plasma polymerization of 1,1-difluoroethene. Journal of Power Sources, 1993, 44, 377-383.	4.0	41
362	Ionically conductive thin polymer films prepared by plasma polymerization, part 9: Vapor-phase preparation of solid polymer electrolytes composed of plasma polymer and lithium trifluoromethanesulfonate. Polymers for Advanced Technologies, 1993, 4, 188-193.	1.6	2
363	Preparation of Thin Cationâ€Exchanger Films from Benzenesulfonyl Fluoride by Glow Discharge Plasma Processes. Zeitschrift Fur Elektrotechnik Und Elektrochemie, 1993, 97, 625-629.	0.9	10
364	Preparation of Thin Cation-Exchange Membranes for Redox-Flow Battery using Glow-Discharge Plasma Process. Electrochemistry, 1993, 61, 1438-1441.	0.3	3
365	Electrodeposition of thin yttriaâ€stabilized zirconia layers using glowâ€discharge plasma. Journal of Applied Physics, 1992, 72, 1577-1582.	1.1	17
366	Enhancement of Monovalent Cation Perm-Selectivity of Nafion by Plasma-Induced Surface Modification. Chemistry Letters, 1992, 21, 2013-2016.	0.7	12
367	Preparation of thin yttria-stabilized zirconia films by vapor-phase electrolytic deposition. Solid State Ionics, 1992, 58, 345-350.	1.3	25
368	Ionically conductive thin polymer films prepared by plasma polymerization—Part 8. Vapor-phase preparation of solid polymer electrolytes composed of plasma polymer and vapor-deposited lithium iodide complex. Electrochimica Acta, 1992, 37, 1483-1486.	2.6	6
369	Modification of Ion-exchange Membrane Surface by Plasma Processes V. Surface Modification of Nafion by 3- (2-aminoethyl) aminopropyltrimethoxysilane. Electrochemistry, 1992, 60, 462-466.	0.3	2
370	Thin Cationâ€Exchanger Films by Plasma Polymerization of 1,3â€Butadiene and Methyl Benzenesulfonate. Journal of the Electrochemical Society, 1991, 138, 3190-3193.	1.3	22
371	Thin Film Solid‣tate Lithium Batteries Prepared by Consecutive Vaporâ€Phase Processes. Journal of the Electrochemical Society, 1991, 138, 1574-1582.	1.3	18
372	A Novel Ultra-thin Cation-exchange Membrane Prepared by Plasma Polymerization. Chemistry Letters, 1990, 19, 953-954.	0.7	15
373	A Novel Thin Film of Anion Exchanger Prepared by Plasma Polymerization. Chemistry Letters, 1990, 19, 513-514.	0.7	4
374	Modification of an Ion-Exchange Membrane Surface by Plasma Process Part 3: Interfacial Resistance of Monovalent Cation Perm-Selective Membrane from Nafion®. Bulletin of the Chemical Society of Japan, 1990, 63, 2150-2153.	2.0	12
375	Ionically conductive thin polymer films prepared by plasma polymerization. Part 7. Preparation and characterization of solid polymer electrolyte having fixed carboxylic acid groups with single mobile species. Solid State Ionics, 1990, 40-41, 624-627.	1.3	10
376	A New Ultraâ€Thin Fluorinated Cation Exchange Film Prepared by Plasma Polymerization. Journal of the Electrochemical Society, 1990, 137, 3319-3320.	1.3	24
377	Material Properties of Spinâ€on Silicon Oxide (SOX) for Fully Recessed NMOS Field Isolation. Journal of the Electrochemical Society, 1990, 137, 229-234.	1.3	4
378	Modification of Ion Exchange Membrane Surface by Plasma Process: I . H+ Ion Perm‧elective Membrane from Nafion for Redoxâ€Flow Battery. Journal of the Electrochemical Society, 1990, 137, 1430-1435.	1.3	29

#	Article	IF	CITATIONS
379	Modification of ion-exchange membrane surface by plasma process. Part 2. Monovalent cation permselective membrane from perfluorosulfonate cation exchange membrane. Journal of Membrane Science, 1990, 54, 163-174.	4.1	17
380	Preparation of ionically conductive thin polymer films by low temperature plasma process Membrane, 1990, 15, 288-295.	0.0	0
381	Enhancement of Proton Selectivity of Cation Exchange Membrane by Plasma Modification. Journal of the Electrochemical Society, 1989, 136, 1247-1248.	1.3	22
382	Ionically Conductive Thin Polymer Film Prepared by Plasma Polymerization: I . Hybrid Film of Plasma Polymer Formed from Octamethylcyclotetrasiloxane, Poly(propylene oxide), and Lithium Perchlorate. Journal of the Electrochemical Society, 1989, 136, 625-630.	1.3	25
383	Preparation and characterization of a thin film of polymer electrolyte by plasma CVD part IV. All-solid-state lithium batteries. Journal of Power Sources, 1989, 26, 457-460.	4.0	10
384	Ionically conductive thin polymer films prepared by plasma polymerization. Part 6. Plasma-parameter-dependent characteristics of solid polymer electrolytes composed of plasma polymerized tris(2-methoxyethoxy) vinylsilane-lithium perchlorate hybrids. Solid State Ionics, 1989, 35, 417-423.	1.3	15
385	Preparation of ultra-thin solid-state lithium batteries utilizing a plasma-polymerized solid polymer electrolyte. Journal of the Chemical Society Chemical Communications, 1989, , 1673.	2.0	9
386	A novel thin film of a solid polymer electrolyte composed of plasma-polymerized tris(2-methoxyethoxy)vinyIsilane–LiClO4hybrid. Journal of the Chemical Society Chemical Communications, 1989, , 358-359.	2.0	7
387	Thin Allâ€Solidâ€State Lithium Batteries Utilizing Solid Polymer Electrolyte Prepared by Plasma Polymerization. Journal of the Electrochemical Society, 1988, 135, 2649-2650.	1.3	15
388	A New Ultra-thin Film of Solid Polymer Electrolyte Prepared by Plasma Polymerization. Chemistry Letters, 1988, 17, 1811-1814.	0.7	3
389	Quadruple perovskite oxides CaMn7O12 proceed by twoâ€activeâ€site reaction mechanism for oxygen evolution reaction. ChemElectroChem, 0, , .	1.7	5